Thermal Science and Engineering 2024, 7(1), 6267.
https://doi.org/10.24294/tse.v7i1.6267

Article

Theoretical investigation on Rh(III)-catalyzed switchable C–H alkenylation of enamide with enone and Rh(I)-catalyzed decarbonylative version of 1,2,3,4-tetrahydroquinoline with anhydride

Nan Lu*, Chengxia Miao, Xiaozheng Lan

College of Chemistry and Material Science, Shandong Agricultural University, Taian 271018, China
*** Corresponding author:** Nan Lu, lun@sdau.edu.cn

CITATION

Lu N, Miao C, Lan X. Theoretical investigation on Rh(III)-catalyzed switchable C–H alkenylation of enamide with enone and Rh(I)-catalyzed decarbonylative version of 1,2,3,4-tetrahydroquinoline with anhydride. Thermal Science and Engineering. 2024; 7(1): 6267. https://doi.org/10.24294/tse.v7i1.6267

ARTICLE INFO

Received: 7 May 2024
Accepted: 21 May 2024
Available online: 1 July 2024

Abstract: The mechanism is investigated for Rh(III)-catalyzed C-H alkenylation of enamide with enone and Rh(I)-catalyzed decarbonylative version of 1,2,3,4-tetrahydroquinoline with anhydride. The former contains β-C(sp^2)−H activation of enamide, 1,2-migratory insertion of enone, β-hydride elimination or protodemetalation with additional HCl. The diastereoselectivity is kinetically controlled favoring alkenylation N-(2Z,4E)-butadiene while the regio-divergence is switchable to alkylation. The latter is composed of rate-limiting oxidative addition of anhydride to Rh(I), C8-selective C–H activation after ligand exchange producing $tBuCO_2H$ and six-membered rhodacycle, decarbonylation releasing CO as new carboxylate ligand and reductive elimination of Rh-alkenyl precursor leading to C8-alkenylated product. The whole process with huge heat release is favorable thermodynamically and all barriers capable to overcome under microwave assistance. The positive solvation effect is suggested by decreased absolute and activation energies in solution compared with in gas. These results are supported by Multiwfn analysis on FMO composition of specific TSs, and MBO value of vital bonding, breaking.

Keywords: C–H alkenylation; regioselectivity; decarbonylation; 1,2-migratory insertion; rhodacyclic

1. Introduction

As important natural products and bioactive molecules, enamides are widely used to be efficient intermediates in organic synthesis. Among many attractive features, the most sought-after field is direct olefinic β-C(sp^2)−H functionalization including alkylation [1–3] and alkenylation [4]. The alkyl radicals were often featured with E-stereoselectivity in alkylation while activated alkenes were coupling partners in alkenylation. Thus C−C bond generation catalyzed by transition metal via C−H activation has received wide interest in recent years. Wherein rhodium(III) catalysts aroused extensive concern with unique advantages as reviewed in reaction assisted by removable directing group [5] and direct C−H arylation of various acyclic enamides with arylsilane [6]. Another interesting aspect is strategies with allylic alcohols in C−H activation through regulation of organometallic selectivity reactivity [7,8]. Recently, many C−H alkylation and alkenylation with allylic alcohols have been achieved for various substrates using rhodium catalyst [9,10].

On the other hand, 1,2,3,4-tetrahydroquinolines are vital active molecules biologically and important compounds pharmacologically. Many efforts were devoted to C–H activation or functionalization of 1,2,3,4-tetrahydroquinolines in past few decades. Particularly in the presence of palladium, rhodium catalysts, the

regioselective alkylation [11,12] can be enabled via introduction of N-directing group. Shi [11] reported aromatic C-H bond activation directed by an N-alkyl acetamino group. Jiang [12] achieved direct synthesis of 8-aryl tetrahydroquinolines via ortho-arylation of arylureas in water. The arylation [13,14] was also available such as Wang's direct C7 allylation of indolines via sequential C–H and C–C activation and Yang's C8-selective C−H alkenylation and alkylation with styrenes and allylic alcohols. The Rh(I)-catalyzed decarbonylative alkeynlation of 1-(pyridine-2-yl)-1,2,3,4-tetrahydroquinoline with cinnamic anhydride was obtained by Zhang [15]. Mohit Kumar reported four examples of Ru(II)-catalyzed C8–H alkenylation of N-Piv-1,2,3,4-tetrahydroquinoline with internal alkynes [16]. However, these advances still have limits in substrate generality and functional group tolerance. Then diverse carboxylic acids demonstrated as advantageous coupling reagents appeared in transition metal-catalyzed decarboxylative and decarbonylative coupling reaction [17–19]. The use of alkenyl carboxylic acids as alkenyl sources in decarbonylative alkenylation received much attention.

Many advantages have been shown for alkenyl C(sp^2)−H functionalization [20]. Based on novel rhodium(III)-catalyzed tunable C4 alkylation and alkenylation of indoles developed by Punniyamurthy [21] and persistent attention on enamides, a breakthrough was Luo's rhodium(III)-catalyzed β-C(sp^2)−H alkenylation and alkylation of acyclic enamides with allyl alcohols [22]. Compared with this was decarbonylative functionalization of (hetero)arene C-H bonds depending on C2-selective C–H alkenylation and polyenylation of imidazoles and directed trideuteromethylation with CD_3CO_2D of Walsh group [23,24]. Especially their Rh(I)-catalyzed C8-selective C–H alkenylation of N-(pyrimidin-2-yl)-1,2,3,4-tetrahydroquinolines [25]. Although excellent regioselectivity and stereoselectivity was achieved, there is no report about detailed mechanistic study explaining the origin of critical step. How the N-(2Z,4E)-butadiene and (Z)-β-C(sp^2)−H alkylated enamide presented in switchable mode under the promotion of rhodium(III)? Why the catalytic activity of rhodium(I) strongly influenced by installable and removable N-directing group? To solve these puzzled problems in experiment, an in-depth theoretical study was necessary for these strategy leading to diverse functionalized enamides and C8-alkenylated and arylated 1,2,3,4-tetrahydroquinolines.

2. Computational details

The geometry optimizations were performed at the B3LYP/BSI level with the Gaussian 09 package [26,27]. The mixed basis set of LanL2DZ for Rh and 6-31G(d) for non-metal atoms [28–32] was denoted as BSI. Different singlet and multiplet states were clarified with B3LYP and ROB3LYP approaches including Becke's three-parameter hybrid functional combined with Lee−Yang−Parr correction for correlation [33–39]. The nature of each structure was verified by performing harmonic vibrational frequency calculations. Intrinsic reaction coordinate (IRC) calculations were examined to confirm the right connections among key transition-states and corresponding reactants and products. Harmonic frequency calculations were carried out at the B3LYP/BSI level to gain zero-point vibrational energy (ZPVE) and thermodynamic corrections at 373 K, 413 K and 1 atm for each

structure in THF and 1,4-Dioxane. The solvation-corrected free energies were obtained at the B3LYP/6-311++G(d,p) (LanL2DZ for Rh) level by using integral equation formalism polarizable continuum model (IEFPCM) in Truhlar's "density" solvation model [40–42] on the B3LYP/BSI-optimized geometries.

As an efficient method obtaining bond and lone pair of a molecule from modern ab initio wave functions, NBO procedure was performed with Natural bond orbital (NBO3.1) to characterize electronic properties and bonding orbital interactions [43,44]. The wave function analysis was provided using Multiwfn_3.7_dev package [45] including research on frontier molecular orbital (FMO) and Mayer bond order (MBO).

3. Results and discussion

The mechanism was explored for (a) Rh(III)-catalyzed switchable C-H alkenylation of enamide 1 with enone 2 leading to N-(2Z,4E)-butadiene 3 and (Z)-β-C(sp^2)−H alkylated enamide 4. (b) Rh(I)-catalyzed decarbonylative alkenylation of 1,2,3,4-tetrahydroquinoline 5 with anhydride 6 producing C8-alkenylated 1,2,3,4-tetrahy-droquinoline 7 (**Scheme 1**). Illustrated by black arrow of **Scheme 2a**, a rhodacyclic intermediate i2 is generated by the reaction of 1 with model catalyst Cp*$RhCl_2$ via chelation assistance through β-C(sp^2)−H activation. After the leaving of HCl, the coordination of enone 2 to i2 and succeeding 1,2-migratory insertion formed intermediate C with loose eight-membered ring and rigorous four-membered ring. From C, the subsequent β-hydride elimination affords alkenylated product 3 along with Cp*Rh(I) and another HCl (red arrow). Alternatively, C can undergo protodemetalation with an additional HCl to give alkylated product 4 and recovered Cp*Rh(III) (green arrow). The alkenylated 3 could be further converted into alkylated 4.

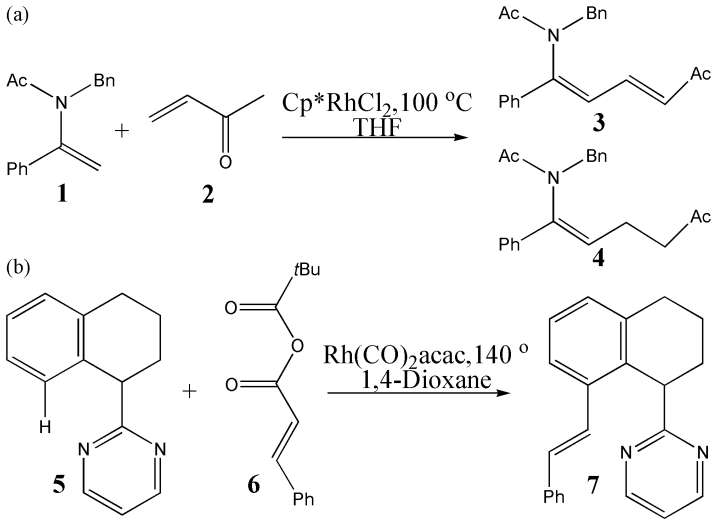

Scheme 1. (a) Rh(III)-catalyzed switchable C-H alkenylation of enamide 1 with enone 2 leading to N-(2Z,4E)-butadiene 3 and (Z)-β-C(sp^2)−H alkylated enamide 4; **(b)** Rh(I)-catalyzed decarbonylative alkenylation of 1,2,3,4-tetrahydroquinoline 5 with anhydride 6 producing C8-alkenylated 1,2,3,4-tetrahy-droquinoline 7.

Displayed by black arrow of **Scheme 2b**, the oxidative addition of anhydride 6

to model Rh(I) species $Rh(CO)_2acac$ generates intermediate D, from which one CO ligand is exchanged by substrate 5 giving intermediate E. Then, the C8-selective C–H activation of E produces acid $tBuCO_2H$ and six-membered rhodacycle F. The subsequent decarbonylation of F releases CO just serving as the lost carboxylate ligand and delivers Rh-alkenyl precursor in3, which proceeds reductive elimination to liberate product 7 and regenerates catalyst Rh(I) species. The schematic structures of optimized TSs in **Scheme 2** were listed by **Figure 1**. The activation energy was shown in **Table 1** for all steps. Supplementary **Table S9**, **Table S10** provided the relative energies of all stationary points. According to experiment, the Gibbs free energies in THF and 1,4-Dioxane solution phase are discussed here.

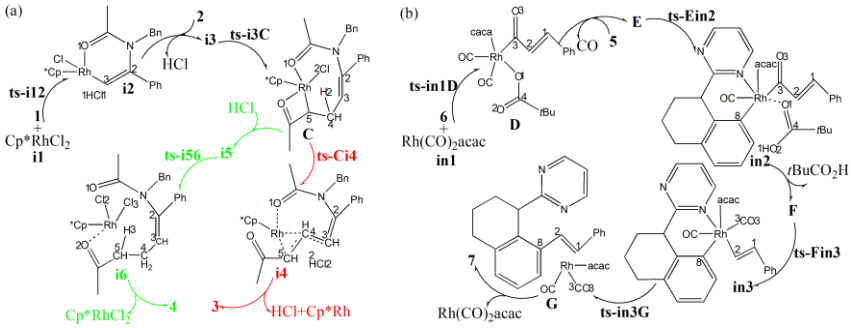

Scheme 2. Proposed reaction mechanism. **(a)** switchable C-H alkenylation of 1 with 2 leading to 3 and 4 catalyzed by Cp^*RhCl_2; **(b)** decarbonylative C–H alkenylation of 5 with 6 producing 7 catalyzed by $Rh(CO)_2(acac)$.
TS is named according to the two intermediates it connects.

Table 1. The activation energy (in kcal mol^{-1}) of all reactions in gas and solvent.

TS	ΔG≠gas	ΔG≠sol
ts-i12	11.12	16.19
ts-i3C	17.63	19.50
ts-Ci4	7.85	9.68
ts-i56	17.92	15.81
ts-in1D	44.14	44.64
ts-Ein2	25.41	25.18
ts-Fin3	40.39	39.60
ts-in3G	8.58	13.62

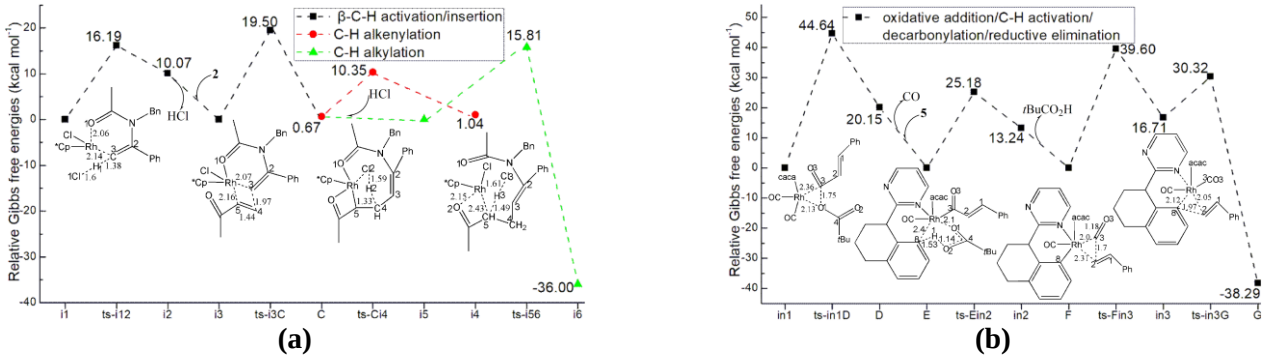

Figure 1. Relative Gibbs free energy profile in solvent phase starting from complex. **(a)** i1, i3, i5; **(b)** in1, E, F.
Bond lengths of optimized TSs in Å.

3.1. β-C(sp^2)−H activation/1,2-migratory insertion/C−H alkenylation

The reaction of 1 with Cp*$RhCl_2$ proceeds via ts-i12 as step 1 with the activation energy of 16.2 kcal mol^{-1} relative to the starting point i1 endothermic by 10.1 kcal mol^{-1} (black dash line of **Figure 1a**). The transition vector includes the approaching of O1 and C3 to Rh slightly ahead of H1 shifting from β-C3 to Cl1 ligand(2.14, 2.06, 1.38, 1.6 Å) (**Figure S1a**). The β-C(sp^2)−H activation assisted by chelation is completed with the formation of rhodacyclic intermediate i2.

Without HCl, a complex i3 from the coordination of enone 2 to i2 is located as another the starting point of next two steps. The 1,2-migratory insertion occurs via ts-i3C with activation energy of 19.5 kcal mol^{-1} in step 2. The transition vector contains concerted bonding of C3 to C4, Rh to C5 and cooperated cleavage of Rh···C3, elongation of C3–C4 (1.97, 2.16, 2.07, 1.44 Å) (**Figure S1b**). The resultant C is characterized by loose eight-membered ring and rigorous four-membered ring with Rh-C5 and Rh-O2 bond as well as sp^3 C4.

The subsequent β-hydride elimination takes place via ts-Ci4 with activation energy of 9.7 kcal mol^{-1} with respect to C in step 3 affords i4 (red dash line of **Figure 1a**). The transition vector corresponds to the depronation of C4 by another Cl ligand (1.33, 1.59 Å) (**Figure S1c**). Once the second HCl and Cp*Rh(I) are departed, alkenylated product (2Z,4E)-3 is obatained at last. Three steps are all readily accessible with mediate barrier from kinetics and unremarkable thermal effects from thermodynamics. Thus 1,2-migratory insertion is determined to be rate-limiting of the whole process.

3.2. C−H alkylation and regioselectivity

Alternatively from C, the intermediate i5 is located binding an additional HCl and taken as starting point of the competitive C−H alkylation (green dash line of **Figure 1a**). This step proceeds via ts-i56 with activation energy of 15.8 kcal mol^{-1} greatly exothermic by −36.0 kcal mol^{-1}. As suggested by the transition vector, the socalled protodemetalation includes de-coordination of Rh···C5 and slightly delayed donating H3 by Cl3 to C5 (2.43, 1.61, 1.49 Å) (**Figure S1d**). After protanation, C5 turns to be sp3 along with the same sp3 C4 in stable final intermediate i6 still with Rh-O2 (2.14 Å) and new Rh-Cl3, which could yield alkylated product 4 and recovered Cp*Rh(III).

Clearly, via comparison between barriers of ts-Ci4 and ts-i56 (9.7, 15.8 kcal mol^{-1}), the excellent diastereoselectivity in experiment is kinetically controlled favoring C–H alkenylation. However, this regio-divergence is switchable considering the relative stability of i4 and i6 (1.0, −36.0 kcal mol^{-1}). Thermodynamically, the alkenylation could be further converted alkylation.

To highlight the idea of feasibility for changes in electron density and not molecular orbital interactions are responsible of the reactivity of organic molecules, quantum chemical tool Multiwfn was applied to analyze of electron density such as MBO results of bonding atoms and contribution of atomic orbital to HOMO of typical TSs (**Table S11**, **Figure S2**). These results all confirm the above analysis.

3.3. Oxidative addition/C8-selective C–H activation

Seen from black dash line of **Figure 1b**, the starting point is located as in1 binding anhydride 6 and $Rh(CO)_2acac$, from which the oxidative addition occurs via ts-in1D with activation energy of 44.6 kcal mol^{-1} endothermic by 20.2 kcal mol^{-1} generating D in step 1. The transition vector indicates the cleavage of anhydride bond C3-O1 and almost simultaneous coordination of C3, O1 to Rh (1.75, 2.36, 2.13 Å) (**Figure S1e**). As Rh(III) intermediate, the resultant D is reactive, from which the ligand exchange is easy from one CO to substrate 5 giving E with Rh-N bond taken as new starting point of next step.

Via ts-Ein2, the C8-selective C-H activation of E proceeds with the activation energy of 25.2 kcal mol^{-1} relative to E endothermic by 13.2 kcal mol^{-1} in step 2. This detailed motion can be demonstrated by the transition vector of ts-Ein2 (**Figure S1f**). That is H1 transferring from C8 to O2 and concerted closing of Rh to C8 (1.53, 1.14, 2.4 Å). The Rh-O1 coordination becomes weak yet still existing (2.1 Å). Therefore a six-membered rhodacycle F is produced with stable Rh-N and Rh-C8 bond after the leaving of $tBuCO_2H$ acid from in2.

3.4. Decarbonylation/reductive elimination

Initiated from F, the following decarbonylation happens via ts-Fin3 in step 3 with a barrier of 39.6 kcal mol^{-1} endothermic by 16.7 kcal mol^{-1} delivering in3 as a Rh-alkenyl precursor. The transition vector is composed of remarkable C2⋯C3 fracture and Rh-C2 bonding (1.7, 2.31 Å) (**Figure S1g**). Comparatively, the single Rh-C3 bond remains strong together with the shortening of C3–O3 from double to triple (2.0, 1.18 Å). This denotes the release CO can just serve as the new carboxylate ligand of Rh(III).

Subsequently, the reductive elimination of in3 takes place via ts-in3G with activation energy of 13.6 kcal mol^{-1} forming G exothermic by −38.3 kcal mol^{-1} in step 4. According to the transition vector, the Rh⋯C2, Rh⋯C8 are breaking and C2–C8 is linking (2.05, 2.12, 1.97Å) (**Figure S1h**). Once the bonding site of C2 is handed over from Rh to C8, the formal single C2–C8 bond reveals the accomplish of final alkenylation. G is rather stable attributed to the binding of regenerated $Rh(CO)_2acac$ and C8-alkenylate product 7.

The oxidative addition is determined to be rate-limiting. Although the barriers of step 1 and step 3 are somewhat high, they are both capable to overcome under the microwave assistance in experiment 140 ℃. Furthermore, the temporary heat absorption due to the production of intermediates with reactive Rh(III) species converts to huge heat release at last with recovered Rh(I) species. Thankfully, the whole process is favorable thermodynamically.

4. Conclusions

Our DFT calculations provide the first theoretical investigation on Rh(III)-catalyzed switchable C-H alkenylation of enamide with enone. The rhodacyclic intermediate is generated through β-$C(sp^2)$−H activation of enamide with Cp^*RhCl_2. After the leaving of first HCl, the 1,2-migratory insertion of enone forms intermediate with loose eight-membered ring and rigorous four-membered ring. The

subsequent β-hydride elimination affords N-(2Z,4E)-butadiene along with Cp*Rh(I) and second HCl. Alternatively with additional HCl, protodemetalation could give (Z)-β-C(sp^2)−H alkylated enamide and recovered Cp*Rh(III). The diastereoselectivity is kinetically controlled favoring alkenylation while the regio-divergence is switchable with alkenylation converted alkylation thermodynamically.

For Rh(I)-catalyzed decarbonylative alkenylation of 1,2,3,4-tetrahydroquinoline with anhydride, the rate-limiting step is initial oxidative addition of anhydride to $Rh(CO)_2$acac. After the ligand exchange from one CO to 1,2,3,4-tetrahydroquinoline, the C8-selective C–H activation produces acid $tBuCO_2H$ and six-membered rhodacycle. The subsequent decarbonylation releases CO serving as new carboxylate ligand and delivers Rh-alkenyl precursor, which proceeds reductive elimination to liberate C8-alkenylated product and regenerated Rh(I). the temporary heat absorption due to the production of intermediates with reactive Rh(III) species converts to at last with recovered Rh(I) species. The whole process with huge heat release is favorable thermodynamically and all barriers capable to overcome under microwave assistance.

The positive solvation effect is suggested by decreased absolute and activation energies in THF and 1,4-Dioxane solution compared with in gas. These results are supported by Multiwfn analysis on FMO composition of specific TSs, and MBO value of vital bonding, breaking.

Author contributions: Conceptualization, NL; methodology, NL; software, NL; validation, NL; formal analysis, NL; investigation, NL; resources, NL; data curation, NL; writing—original draft preparation, NL; writing—review and editing, NL; visualization, NL; supervision, CM; project administration, CM; funding acquisition, XL. All authors have read and agreed to the published version of the manuscript.

Funding: This work was supported by National Natural Science Foundation of China (21973056, 21972079) and Natural Science Foundation of Shandong Province (ZR2019MB050) and Key Laboratory of Agricultural Film Application of Ministry of Agriculture and Rural Affairs, P.R. China.

Conflict of interest: The authors declare no conflict of interest.

References

1. Guo JY, Zhang ZY, Guan T, et al. Photoredox-catalyzed stereoselective alkylation of enamides with N-hydroxyphthalimide esters via decarboxylative cross-coupling reactions. Chemical Science. 2019; 10(38): 8792-8798. doi: 10.1039/c9sc03070k
2. Guo JY, Guan T, Tao JY, et al. Stereoselective C(sp2)–H Alkylation of Enamides with Unactivated Aliphatic Carboxylic Acids via Decarboxylative Cross-Coupling Reactions. Organic Letters. 2019; 21(20): 8395-8399. doi: 10.1021/acs.orglett.9b03169
3. Zhang X, Yang TM, Hu LM, et al. Stereoselective Iron-Catalyzed Alkylation of Enamides with Cyclopropanols via Oxidative C(sp2)–H Functionalization. Organic Letters. 2022; 24(47): 8677-8682. doi: 10.1021/acs.orglett.2c03563
4. Gigant N, Gillaizeau I. Palladium(II)-Catalyzed Direct Alkenylation of Nonaromatic Enamides. Organic Letters. 2012; 14(13): 3304-3307. doi: 10.1021/ol301249n
5. Rej S, Chatani N. Rhodium-Catalyzed C(sp2)- or C(sp3)−H Bond Functionalization Assisted by Removable Directing Groups. Angewandte Chemie International Edition. 2019; 58(25): 8304-8329. doi: 10.1002/anie.201808159
6. Li X, Sun K, Shen W, et al. Rhodium(III)-Catalyzed Direct C–H Arylation of Various Acyclic Enamides with Arylsilanes. Organic Letters. 2020; 23(1): 31-36. doi: 10.1021/acs.orglett.0c03578

7. Singh D, Kumar GS, Kapur M. Oxazolinyl-Assisted Ru(II)-Catalyzed C–H Allylation with Allyl Alcohols and Synthesis of 4-Methyleneisochroman-1-ones. The Journal of Organic Chemistry. 2019; 84(20): 12881-12892. doi: 10.1021/acs.joc.9b01536
8. Kumar GS, Chand T, Singh D, et al. Ruthenium-Catalyzed C–H Functionalization of Benzoic Acids with Allyl Alcohols: A Controlled Reactivity Switch between C–H Alkenylation and C–H Alkylation Pathways. Organic Letters. 2018; 20(16): 4934-4937. doi: 10.1021/acs.orglett.8b02064
9. Nipate DS, Meena N, Swami PN, et al. Rh(iii)-catalyzed oxidative [4+2] annulation of 2-arylquinoxalines and 2-aryl-2H-indazoles with allyl alcohols. Chemical Communications. 2024; 60(3): 344-347. doi: 10.1039/d3cc04600a
10. Khake SM, Chatani N. Rhodium(III)-Catalyzed Oxidative C–H Alkylation of Aniline Derivatives with Allylic Alcohols To Produce β-Aryl Ketones. ACS Catalysis. 2022; 12(8): 4394-4401. doi: 10.1021/acscatal.2c00854
11. Shi Z, Li B, Wan X, et al. Suzuki–Miyaura Coupling Reaction by PdII-Catalyzed Aromatic C–H Bond Activation Directed by an N-Alkyl Acetamino Group. Angewandte Chemie International Edition. 2007; 46(29): 5554-5558. doi: 10.1002/anie.200700590
12. Jiang Z, Zhang L, Dong C, et al. Direct synthesis of 8-aryl tetrahydroquinolines via pd-catalyzed ortho-arylation of arylureas in water. RSC Adv. 2013; 3(4): 1025-1028. doi: 10.1039/c2ra22901c
13. Wang Q, Shi L, Liu S, et al. Solvent-free and room temperature microwave-assisted direct C7 allylation of indolines via sequential C–H and C–C activation. RSC Advances. 2020; 10(18): 10883-10887. doi: 10.1039/d0ra02016h
14. Yang J, Chen C, Zhao H, et al. Rhodium(III-Catalyzed C8-Selective C−H Alkenylation and Alkylation of 1, 2, 3, 4-Tetrahydroquinolines with Styrenes and Allylic Alcohols. Advanced Synthesis & Catalysis. 2023; 365(7): 1027-1035. doi: 10.1002/adsc.202300074
15. Zhang L, Chen C, Han J, et al. Ru-Catalyzed selective C–H oxidative olefination with N-heteroarenes directed by pivaloyl amide. Organic Chemistry Frontiers. 2016; 3(10): 1271-1275. doi: 10.1039/c6qo00327c
16. Mohit Kumar R, Khan AA, et al. Ru(II)-Catalyzed Regioselective Hydroarylative Coupling of Indolines with Internal Alkynes by C−H Activation. European Journal of Organic Chemistry. 2021; 2021(14): 2107-2113. doi: 10.1002/ejoc.202100085
17. Wei Y, Hu P, Zhang M, et al. Metal-Catalyzed Decarboxylative C–H Functionalization. Chemical Reviews. 2017; 117(13): 8864-8907. doi: 10.1021/acs.chemrev.6b00516
18. Schwarz J, König B. Decarboxylative reactions with and without light – a comparison. Green Chemistry. 2018; 20(2): 323-361. doi: 10.1039/c7gc02949g
19. Dzik WI, Lange PP, Gooßen LJ. Carboxylates as sources of carbon nucleophiles and electrophiles: comparison of decarboxylative and decarbonylative pathways. Chemical Science. 2012; 3(9): 2671. doi: 10.1039/c2sc20312j
20. Li X, Luo H, Song R, et al. Selective Cross-Dehydrogenative Coupling of Various Acyclic Enamides with Heteroarenes via Rh(III)-Catalyzed C–H Activation. Organic Letters. 2023; 25(28): 5262-5267. doi: 10.1021/acs.orglett.3c01786
21. Pradhan S, Mishra M, De PB, et al. Weak Coordination Enabled Switchable C4-Alkenylation and Alkylation of Indoles with Allyl Alcohols. Organic Letters. 2020; 22(5): 1720-1725. doi: 10.1021/acs.orglett.9b04612
22. Li X, Liu J, Song R, et al. Rhodium(III)-Catalyzed Switchable β-C(sp2)–H Alkenylation and Alkylation of Acyclic Enamides with Allyl Alcohols. Organic Letters. 2024; 26(17): 3673-3678. doi: 10.1021/acs.orglett.4c01234
23. Zhao H, Luo Z, Yang J, et al. Ligand-Promoted RhI-Catalyzed C2-Selective C−H Alkenylation and Polyenylation of Imidazoles with Alkenyl Carboxylic Acids. Chemistry – A European Journal. 2022; 28(36). doi: 10.1002/chem.202200441
24. Zhao H, Zeng Q, Yang J, et al. Rhodium(i)-catalyzed directed trideuteromethylation of (hetero)arene C–H bonds with CD3CO2D. Organic & Biomolecular Chemistry. 2022; 20(38): 7645-7649. doi: 10.1039/d2ob01581a
25. Zhao H, Zeng Q, Yang J, et al. Microwave-assisted Rhodium(I)-Catalyzed C8-Regioselective C−H Alkenylation and Arylation of 1,2,3,4-Tetrahydroquinolines with Alkenyl and Aryl Carboxylic Acids. Advanced Synthesis & Catalysis. 2024; 366(8): 1820-1826. doi: 10.1002/adsc.202400053
26. Frisch MJ, Trucks GW, Schlegel HB, et al. Gaussian 09 (Revision B.01). Gaussian Inc; 2010.
27. Hay PJ, Wadt WR. Ab initio effective core potentials for molecular calculations-potentials for the transition-metal atoms Sc to Hg. The Journal of Chemical Physics. 1985; 82: 270-283.
28. Lv H, Han F, Wang N, et al. Ionic Liquid-Catalyzed C−C Bond Formation for the Synthesis of Polysubstituted Olefins. European Journal of Organic Chemistry. 2022; 2022(45). doi: 10.1002/ejoc.202201222
29. Zhuang H, Lu N, Ji N, et al. Bu4NHSO4-Catalyzed Direct N-Allylation of Pyrazole and its Derivatives with Allylic

Alcohols in Water: A Metal-Free, Recyclable and Sustainable System. Advanced Synthesis & Catalysis. 2021; 363(24): 5461-5472. doi: 10.1002/adsc.202100864

30. Lu N, Lan X, Miao C, et al. Theoretical investigation on transformation of Cr(II) to Cr(V) complexes bearing tetra-N-heterocyclic carbene and group transfer reactivity. International Journal of Quantum Chemistry. 2020; 120(18). doi: 10.1002/qua.26340
31. Lu N, Liang H, Qian P, et al. Theoretical investigation on the mechanism and enantioselectivity of organocatalytic asymmetric Povarov reactions of anilines and aldehydes. International Journal of Quantum Chemistry. 2020; 120: e26574.
32. Lu N, Wang Y. Alloy and Media Effects on the Ethanol Partial Oxidation Catalyzed by Bimetallic Pt6M (M = Co, Ni, Cu, Zn, Ru, Rh, Pd, Sn, Re, Ir, and Pt). Computational and Theoretical Chemistry. 2023; 1228: 114252.
33. Becke AD. Density-functional thermochemistry. IV. A new dynamical correlation functional and implications for exact-exchange mixing. The Journal of Chemical Physics. 1996; 104(3): 1040-1046. doi: 10.1063/1.470829
34. Lee C, Yang W, Parr RG. Development of the Colle-Salvetti correlation-energy formula into a functional of the electron density. Physical Review B. 1988; 37(2): 785-789. doi: 10.1103/physrevb.37.785
35. Catellani M, Mealli C, Motti E, et al. Palladium−Arene Interactions in Catalytic Intermediates: An Experimental and Theoretical Investigation of the Soft Rearrangement between η1 and η2 Coordination Modes. Journal of the American Chemical Society. 2002; 124(16): 4336-4346. doi: 10.1021/ja016587e
36. Zicovich-Wilson CM, Pascale F, Roetti C, et al. Calculation of the vibration frequencies of α-quartz: The effect of Hamiltonian and basis set. Journal of Computational Chemistry. 2004; 25(15): 1873-1881. doi: 10.1002/jcc.20120
37. Nielsen RJ, Goddard WA. Mechanism of the Aerobic Oxidation of Alcohols by Palladium Complexes of N-Heterocyclic Carbenes. Journal of the American Chemical Society. 2006; 128(30): 9651-9660. doi: 10.1021/ja060915z
38. Zandler ME, D'Souza F. The remarkable ability of B3LYP/3-21G(*) calculations to describe geometry, spectral and electrochemical properties of molecular and supramolecular porphyrin–fullerene conjugates. Comptes Rendus Chimie. 2006; 9(7-8): 960-981. doi: 10.1016/j.crci.2005.12.008
39. Marenich AV, Cramer CJ, Truhlar DG. Universal Solvation Model Based on Solute Electron Density and on a Continuum Model of the Solvent Defined by the Bulk Dielectric Constant and Atomic Surface Tensions. The Journal of Physical Chemistry B. 2009; 113: 6378-6396. doi: 10.1021/jp810292n
40. Tapia O. Solvent effect theories: Quantum and classical formalisms and their applications in chemistry and biochemistry. Journal of Mathematical Chemistry. 1992; 10: 139-181.
41. Tomasi J, Persico M. Molecular Interactions in Solution: An Overview of Methods Based on Continuous Distributions of the Solvent. Chemical Reviews. 1994; 94: 2027-2094.
42. Tomasi J, Mennucci B, Cammi R. Quantum Mechanical Continuum Solvation Models. Chemical Reviews. 2005; 105: 2999-3093.
43. Reed AE, Weinstock RB, Weinhold F. Natural population analysis. The Journal of Chemical Physics. 1985; 83: 735-746.
44. Reed AE, Curtiss LA, Weinhold F. Intermolecular interactions from a natural bond orbital donor-acceptor view point. Chemical Reviews. 1988; 88: 899-926.
45. Lu T, Chen F. Multiwfn: A multifunctional wavefunction analyzer. Journal of Computational Chemistry. 2012; 33: 580-592.